Alternative General Fitting Methods for Real-Time Cell-Count Experimental Data Processing

Juan Alfonso Serrano, Pablo Pérez, Gloria Huertas, and Alberto Yúfera, *Member, IEEE*

***Abstract*—This paper reports two general methods for extraction of cell-electrode electrical model parameters in cell culture (CC) assays. The presented approaches can be applied to CC assays based on electrical cell-substrate impedance spectroscopy (ECIS) technique for real-time supervision, providing the cell number per square centimeter, i.e., the cell density, as main result. Both of the proposed methods - minimization of system equations and data predictive model - search, during the experiment, the optimum values of the electrical model parameters employed for the electrode-cell model. The results of this search enable a fast and efficient calculation of the involved cell-electrode model parameters and supply real-time information on the cell number. For the sake of experimental validation, we applied the proposed methods to practical CCs in cell growth assays with a cell line of AA8 Chinese hamster ovarian fibroblasts and the Oscillation Based Test technique for bioimpedance measurements. These methods can be easily extrapolated to any general cell lines and/or other bioimpedance test methodologies.**

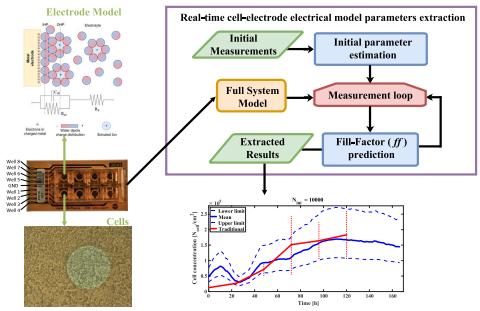

***Index Terms*—Bioimpedance, cell-culture, ECIS, electrical electrode model, OBT.**

I. Introduction

MANY biological and medical assays are based on the preparation of a cell culture (CC) for a given cell line and then observation of the cell progress over time after applying a given product such as a toxin or a drug, external conditions, a protocol, etc. [1]. This is a common and useful procedure employed in biomedical labs and exploited in fields such as cell biology [2], genetics [3], biochemistry [4], pharmacology [5], tissue engineering [6], immunology [7], and food control [8]. A CC assay requires seeding a number of cells on a substrate, commonly a Petri dish, and applying several conditions or protocols, defined in the context of the assay. To obtain information at a given time instant about the cell status, e.g., their size, number, type, and health, it is generally required to "kill" the cells and fix them [1] for microscope observation. This is why these assays are commonly called "end-point protocols": the CC finishes when its observation is decided. For this reason, CC assays need many parallel preparations in terms of observation points specified in the assay description, requiring subsequent statistical analysis, significant human workload, and many material resources.

To overcome the drawbacks of end-point protocols, Giaever and Keese [9] proposed the so-called Electrical Cell-Substrate Sensing (ECIS) technique as an alternative procedure to perform real-time monitoring of CCs, thereby avoiding multiple samples. This study suggested testing the impedance of a CC when it is positioned between two electrodes (when 4-wires setups are used, the current lines of the applied electric field do not correctly sense the cells). Given that cells are attached to the CC substrate (electrodes), it is possible to have an estimation of the cell number by measuring the bioimpedance between the two electrodes. There results were developed by leveraging prior studies [10]–[13], which demonstrated the feasibility of the impedance-based technique. Practical information reported in most previous ECIS studies includes the growth evolution over time by monitoring the bioimpedance measured between the two electrodes (resistive and capacitive components) from cell seeding to confluence

This work was supported in part by the Spanish Government's, Ministerio de Ciencia, Innovacióny Universidades and in part by the Plan Estatal 2017–2020 Retos: Real Time Monitoring of Hemodynamic Variables Using Intelligent Stents (iSTENT) with Capaci-tive Sensors and Bioimpedance, co-financed with FEDER under Project RTI2018-093512-B-C21. The associate editor coordinating the review of this article and approving it for publication was Dr. Shanhong Xia. *(Corresponding author: Juan Alfonso Serrano.)*

Juan Alfonso Serrano, Pablo Pérez, and Alberto Yúfera are with the Departamento de Tecnología Electrónica, ETSII, Universidad de Sevilla, 41012 Seville, Spain, and also with the Instituto de Microelectrónica de Sevilla (IMSE-CNM-CSIC), 41092 Sevilla, Spain (e-mail: serrano@imse-cnm.csic.es; pablopg@imse-cnm.csic.es; yufera@imse-cnm.csic.es).

Gloria Huertas is with the Departamento de Electrónica y Electromagnetismo, Facultad de Física, Universidad de Sevilla, 41012 Seville, Spain, and also with the Instituto de Microelectrónica de Sevilla (IMSE-CNM-CSIC), 41092 Sevilla, Spain (e-mail: gloria@imse-cnm.csic.es).

(electrode surface full of cells) phases. These data are reliable for CC characterization and have been useful for biomedical teams. However, the evolution of the cell numbers over time has not been reported. The key to access this information relies on the knowledge of the electrical model for the electrode-cell system, which is mandatory for decoding the electrical bioimpedance measurements.

The first proposal for an electrode-cell electrical model was described in [10]. This approach considered the cell culture as a monolayer and obtained the solution of Maxwell's equations for the electrical field in the electrode-cell interface. To find the solution, parameter values such as R_b (barrier resistance between cells), h (electrode-cell interface distance), and r (cell radius) were proposed and selected to fulfill the equations derived. In a subsequent study, Huang *et al.* [14], considered a single cell on top of an electrode and extracted the electrical performance of the system by simulating its electrical response to an AC signal with finite-element simulation tools. A new resistance R_{gap} – the so-called gap resistance –was incorporated to the electrode-cell electrical model that represented the obstruction to the electrical current flowing along the electrode-cell interface, which usually extends several nanometers. They also included a geometrical parameter *ff* – the so-called *fill factor* – that described the percentage of electrode area covered by the cells. Other approaches [15] employs a RC model to evaluate the load response associated to cells, as suggested in [10], without considering their size or any other cell properties. Recently, a novel approach [16] was proposed to employ the model in [14] with empirical parameter fitting, modifying the dependence of R_s – the so-called spreading resistance – on *ff*. This dependence may be due to changes in extracellular composition during the experiment. The main conclusions in this study were that electrode mismatch precluded the use of the same parameter values for the electrode-electrical model, requiring evaluation for each sample or CC. The electrode impedance was observed to evolve over time throughout the assay (several days in this case). In addition, it was necessary to wait until the confluence phase of the CC to apply the proposed fitting model.

The present study proposes the use of empirical data for electrode-cell electrical model calculations as in [16], but incorporating only the initial data measurements of the CC assay and calculating the electrode-cell parameter values for calibration. Herein, we propose two approaches to find the values of the parameters in the electrical model in real time. The first one is based on the analytical solution of the electrical response obtained by minimization of system equations (*MSE*). The parameter values are provided from the equations that describe the system solution. As an example, we applied the Oscillation Based Test (*OBT*) method to measure the system bioimpedance.

Machine Learning (ML) algorithms are increasingly relevant to data science and experimental data from bioimpedance sensing is not an exception. The application of ML algorithms to analyze bioimpedance cell measurements has been previously evaluated by the authors [17]. Following this idea, the second method searches for the best-fitting parameter values from a design space generated by moving the corresponding cell-electrode electrical parameter within a given range while evaluating the parameter proposal using the *OBT* equations. These parameter values are employed for training a k-nearest neighbor (KNN) algorithm [18], which will be applied for data decoding after the calibration phase.

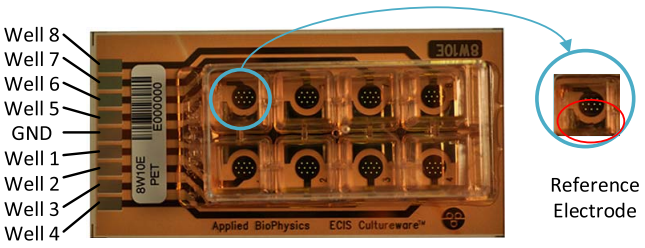

Fig. 1. 8E10E commercial electrodes from Applied Biophysics (AB). This is the substrate employed in the CC assays evaluated in this study. Each well contains 10 circular microelectrodes (diameter of 250 μm) connected in parallel and 1 reference electrode (GND).

The article is organized as follows. Section II describes the material and methods, the CC protocol, the electrode-cell electrical model, and the main *OBT* equations employed. Both of the proposed experimental fitting models, i.e., *MSE* and data predictive model (*DPM),* are described in detail in Section III. The main results from the same CC data are reported and compared in Section IV. Finally, conclusions are highlighted in Section V.

II. Materials and Methods

A. Cell-Culture Assay

The experimental assays were based on commercial electrodes provided by AB [2] (Fig. 1). These devices contain eight separated wells, each with ten circular biocompatible gold microelctrodes of 250-μm diameter in parallel for input current, and a large ground electrode for output current. This study was performed using a cell line described next.

The biological sample under test (SUT) was formed by Chinese hamster ovarian fibroblasts. This cell line is identified as AA8 (American Type Culture Collection). This sample was immersed in a McCoy's medium supplemented with 10 % (v/v) foetal calf serum, 2 mM L-glutamine, 50 μg/mL streptomycin, and 50 U/mL penicillin. The growing environment was established at 37 °C and 5 % CO2 in a humid atmosphere. Different initial cell numbers were seeded for our experiments, namely 2.500, 5.000, and 10.000, obtained by dilution of an initially high cell density. Petri-dish cultures were also made with the same cell density for further matching with the proposed bioimpedance (*BioZ*) test.

B. Cell-Electrode Electrical Model

A CC assay was initiated in the aforementioned commercial devices. As pointed out above, the system had eight wells, each with a two-electrode configuration: input and output (Fig. 1). Cells were deployed on the electrodes along with the medium solution. The cell-electrode electrical model describes the behavior of a CC and corresponding electrodes. Fig. 2 shows the electrode model in a saline solution, while Fig. 3 shows

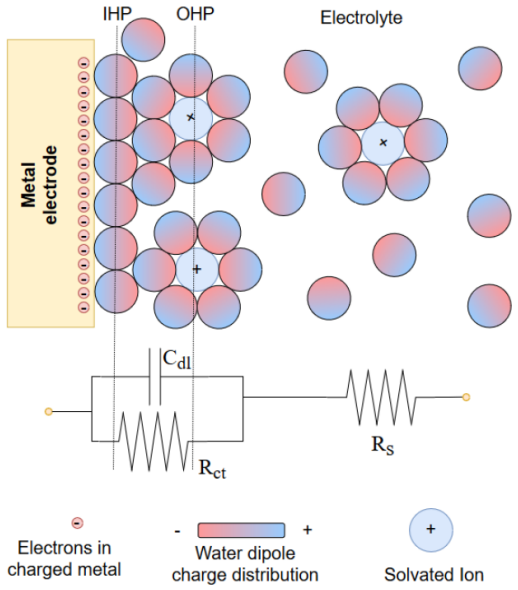

Fig. 2. Electrode electrical model immersed in an ionic solution. A double layer is formed near the electrode; an Inner Helmholtz Plane is defined by the distance at which water dipoles are aligned with the electrode surface. An Outer Helmholtz Plane is defined as the distance at which solvated ions are aligned near the electrode.

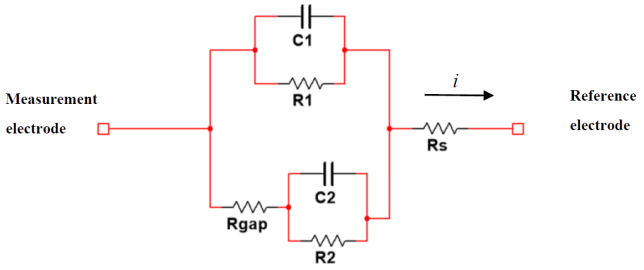

Fig. 3. BioZ electrical model: electrical model of an electrode in a saline solution considering the influence of the cells covering an ff percentage of the electrode area.

its evolution considering the influence of the cells covering an *ff* percentage of the electrode area. This model has been extensively explored in the literature, [9]–[14] and [19]. To test the cell growth over the electrodes, the OBT measurement technique was employed [20]. The sensor system in the OBT architecture forms an oscillator where the biological interface is connected as a load (Z) into the main loop. As a result, a biological sensor is created. The CC assay growth is related to changes in bioimpedance, which generate variations over the amplitude and frequency of the signal generated in the oscillator. The *OBT* technique is just an example. In OBT the central frequency can be tuned by the band pass filter [13], the reactive impedance due to the cell membrane capacitance is very high for the lower frequency spectrum (up to several kHz). The sensor frequency selection ensures that electrical current lines do not pass through the cell. The proposed fitting methods can be easily extrapolated to other measurement techniques.

A previous study [16] described the changes on electrical model parameters and their importance to predict the values of *ff* or cell density in real time, as well as the equations and parameters of the sensor and its configuration to collect data.

The BioZ electrical model shown in Fig. 3 is described by R_{gap}, R_s, and the following parameters:

$$R_1 = \frac{R_{ct}}{(1-ff)} \quad R_2 = \frac{R_{ct}}{ff}$$
$$C_1 = C_{dl} \cdot (1-ff) \quad C_2 = C_{dl} \cdot ff \tag{1}$$

where R_{ct} and C_{dl} are the charge transfer resistance and the double-layer capacitor, respectively [19], modeled in Fig. 2. The parameters R_1, R_2, C_1, and C_2 model the electrical behavior of the microelectrodes covered by the cells. Nodal analysis provides the transfer function that models the *BioZ*:

$$H_z(s) = \frac{k_2 \cdot s^2 + k_1 \cdot \frac{\omega_{0z}}{Q_z} \cdot s + k_0 \cdot \omega_{0z}^2}{s^2 + \frac{\omega_{0z}}{Q_z} \cdot s + \omega_{0z}^2} \tag{2}$$

where,

$$\mathrm{k_2} = R_s \quad \mathrm{k_1} = R_s + \frac{R_{gap} \cdot R_1}{2 \cdot R_{gap} + R_1 + R_2}$$
$$\mathrm{k_0} = R_s + \frac{R_1 \cdot (R_{gap} + R_2)}{R_{gap} + R_1 + R_2}$$
$$\omega_{0z} = \sqrt{\frac{R_{gap} + R_1 + R_2}{R_{gap} \cdot (R \cdot C)^2}} \quad Q_z = \omega_{0z} \frac{R_{gap} \cdot R \cdot C}{2 \cdot R_{gap} + R_1 + R_2} \tag{3}$$

C. OBT System

As mentioned in Section II.A, the measurement method we applied for transforming *BioZ* into a measurable variable was OBT. This is simply a possible technique; any other could be used. The electronic system oscillates at a given amplitude and frequency. These two parameters are defined by the *BioZ* value of the CC and can provide the cell growth information along with a proper knowledge of the sensor electrical model. The oscillation system used to measure *BioZ* was reported in [16]; the same block diagram and parameter values were applied in the present study.

The Barkhausen stability criterion – see below Equation (4) – is the mathematical condition that the closed-loop feedback system must fulfill to obtain sustained oscillations. Thus, the oscillation parameters a_{osc} and f_{osc} can be derived by setting the real and imaginary parts of Equation (4) to 0:

$$1 + H(s = j\varpi) \cdot N(a_{osc}, \varpi_{osc}) = 0 \tag{4}$$

where $\omega_{osc} = 2\pi f_{osc}$, and $H(s = j\omega)$ is the transfer function with no linear element of the *OBT*, which includes the *BioZ*, a band-pass filter, and other electronic elements; $N(a_{osc}, \omega_{osc})$ is the descriptive function of the comparator, that is, the linearized mathematical description of the comparator, whose calculation was described in [20]. Equation (4) will be used as a demonstrative vehicle to show how both fitting methods work; any other system equations could be employed.

III. ESTIMATION METHODS OF REAL-TIME EXPERIMENTAL CELL-CULTURE GROWTH

In this section, the two methods proposed for analysis of the measurements provided by the sensor are compared. Firstly,

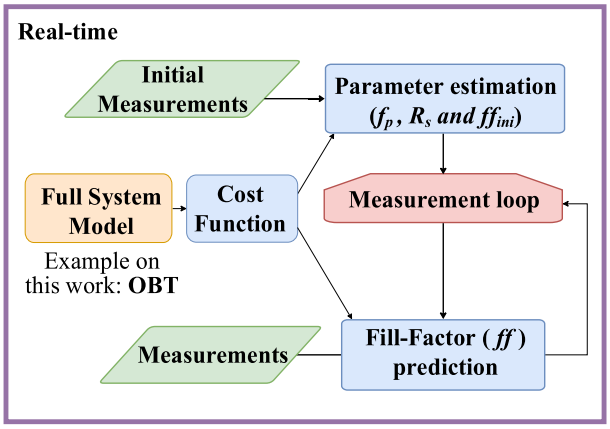

Fig. 4. Flowchart of the MSE method. A cost function is used to estimate R_{si} and f_p from the initials measurements, and R_{gap}, ΔR_s, and ff for each measurement.

minimization of the module of the function in Equation (4), denoted as *MSE*. Secondly, DPM, which is a method based on electrical parameter fitting from initial experimental measures.

Both methods rely on the numerical solution of the dynamic models for the system and the oscillation condition expressed in Equation (4). In particular, the oscillation condition is given by Equation (4), where the real and imaginary parts, denoted as *eq1* and *eq2*, respectively, from now on (defined in the Appendix as Equations (1) and (2), respectively), must be zero.

A. Minimization of System Equations

This method is based on a previous study [16]. Joining *eq1* and *eq2*, derived by setting the real and imaginary parts of Equation (4) to zero, and three parameters derived from the electrochemical interface and the cells under test, namely R_{gap}, ΔR_s, and ff, we have 2 equations and 3 variables. The solution for these equations, as previously reported in [16], is found by setting the values of R_{gap} and ΔR_s through a calibration experiment using a previous cell line, given that these values seem to be specific to each cell line and well type. However, herein, the method is focused on a different approach for the estimation of cell growth; the major advantage of this approach is that it enables estimation with no previous experiments by minimizing a multivariable function with constraints. This function must contain the three unknown variables and meet the oscillation condition defined in Equation (4).

Fig. 4 shows the flow diagram of the *on-line* estimation process. It minimizes a cost function, which is explained below, after each CC measurement to obtain R_{gap}, ΔR_s, and ff. We waited for a few hours at the beginning of the each experiment until R_{si} and f_p, which is one of the poles in Equation (2) used to estimate initial values of R_{ct} and C_{dl}, could be estimated.

Matlab was the environment used to conduct all testing. The *Matlab* function used to minimize the function was *fmincon*, which finds the minimum of a constrained nonlinear multivariable function. The *fmincon* algorithm used was *sqp* [21]. The function to be minimized must ensure that the Barkhausen stability criterion is fulfilled. Therefore, we employed the following function:

$$f(R_{gap}, \Delta R_s, ff) = \sqrt{(eq1^2 + eq2^2)} \tag{5}$$

This function implies that the module of the real and imaginary parts in Equation (4) must be 0. Given that both terms are squared, it is ensured that *eq1* and *eq2* cannot compensate each other to minimize $f(R_{gap}, \Delta R_s, ff)$ to 0. In this way, it is ensured that the Barkhausen stabilization criterion is fulfilled, i.e., *eq1* and *eq2* are 0.

Note that *fmincon* needs a starting value per execution for each variable, as expressed in Equation (6), in addition of possible restrictions (or bounds) of such variables, expressed in Equation (7).

$$ff_n = ff_{n-1} \quad R_{gap} = 500\Omega \quad \Delta R_s = 0\Omega \tag{6}$$

$$\begin{aligned} ff_{bounds} &= \left[0.05\ 0.999\right]\%_1 \\ R_{gap.bounds} &= \left[100\ 2e3\right]\Omega \\ \Delta R_{s.bounds} &= \left[-R_{si}\ 2\cdot R_{si}\right]\Omega \end{aligned} \tag{7}$$

The initial value of ff for each *fmincon* iteration is the value of ff at the previous point of the experiment. The ff limits its value to the range [0,1]. The initial value of R_{gap} for each *fmincon* iteration is 500 Ω. The limits for R_{gap} precludes that it becomes negative and excessively large, that is, its variation is allowed for positive values (negative ones do not make physical sense). The initial value of ΔR_s for each *fmincon* iteration is 0 Ω. The limits imposed on ΔR_s prevent R_s from becoming negative, or too large, but still allow for a wide variation range.

The estimation process is described next. First, it is required to wait for the CC to begin to grow. Then, using the initial values of f_{osc} and a_{osc}, the position of the pole, f_p, as well as the initial values of R_s and R_{si}, are calculated as in [16]. This is achieved by the *fmincon* minimization procedure of the function expressed in Equation (5), using f_p and R_s as unknown variables together with ff (the values of R_{gap} and ΔR_s are the same as in Equation (6), and the initial value of ff is estimated from the initial cell number in each well). This estimation is only computed at the beginning of the experiment, with the initial conditions and bounds provided in Equation (8) below.

$$ff_n = ff_{ini} \quad f_p = 90\text{Hz} \quad R_s = 500\Omega$$

$$\begin{aligned} f_{bounds} &= \left[0.05\ 0.999\right]\%_1 \\ f_{p.bounds} &= \left[0.1\ 1e3\right]\text{Hz} \\ R_{s.bounds} &= \left[0.1\ 2e3\right]\Omega \end{aligned} \tag{8}$$

At this point, it is already possible to estimate the values of R_{gap}, ΔR_s, and ff at any arbitrary point of the experiment through *fmincon*. Interestingly, note that R_{gap} and ΔR_s do not affect the electrode-cell model when $ff \to 0$, that is, at the beginning of the experiment.

B. Dataset Predictive Model

Note that the first proposed method, i.e., MSE, finds the most suitable operation point for the sensor, which corresponds to a certain oscillatory solution. This requires a certain amount of computational power at every iteration.

TABLE I
PARAMETER BOUNDS

Method	R_{ct} $[M\Omega]$	C_{dl} $[nF]$	R_s $[\Omega]$
DPM	0.6 – 2.6	16 – 64	250 – 1000
MSE	0.04 – 0.09	23 – 37	290 – 454

An alternative approach is presented in this section. The DPM method relies on the definition of a full dynamic model for the whole growing process in which the cell-electrode interface is evolving through the experiment; the values for R_s and R_{gap} are not constant in this case.

A certain degree of variance across the different electrodes involved in the experimental setup is assumed. According to Fig. 2, values for C_{dl}, R_{ct}, and R_s can be computed to provide an electrical model from the electrode material and conductive ion concentration in the solution [19]. Nominal values for such parameters are $C_{dl} = 32nF$, $R_{ct} = 1.3\ M\Omega$, and $R_s = 500\Omega$. Fig. 5 shows a general diagram of the *DPM* process. This method requires the computation of a multivariate dataset accounting for the variation of the electrode-model electrical parameters over a certain range (Input Range). Then, a KNN algorithm [18] network is trained using this multivariate dataset to provide the parameters that better fit our experimental data during the calibration step (Electrical Parameter Determination).

Using the electrical parameters computed in the calibration step, a prediction of *ff* values is obtained through a linear regression from the expected *ff* curves for such electrical values. The algorithm steps are described in detail next.

1) Dataset Generation: As described above, the electrode model is a source of significant error in terms of how the electrical parameters contribute to the *ff* estimation. The fact that real electrodes introduce some uncertainty and dispersion across different devices cannot be neglected. To generate a multivariate dataset establishing the relation between *ff* and the electrical model, a range for the electrical parameters is defined. TABLE I reports the ranges of C_{dl}, R_{ct}, and R_s obtained from the *MSE* method.

A numerical simulation was performed using the aforementioned parameters and setting *ff* to zero (initial status). The results are depicted in Fig. 6 and Fig. 7, where the amplitude and frequency sensor output are described for the whole multivariate range. The contribution arising from R_{ct} to the frequency and amplitude curves is almost negligible. This is why we present R_{ct} and C_{dl} as the dependent variables.

2) KNN Training and Prediction: Training a *KNN Network* using the previously described dataset enables the prediction of the closest point to a given output value from the sensor (a_{osc} and f_{osc}) over the early stage of the experiment. The *KNN* algorithm provides the most suitable fitting for the electrical model that corresponds to the experimental data acquired over the initial period ($ff \to 0$).

3) Fill Factor (Ff) Estimation: At this point, the electrical model parameters are known, thus enabling the calculation of *ff* from the electrical model. The analysis of the frequency and amplitude curves in terms of *ff* already revealed a nearly linear behavior [11]. Hence, to estimate the value of *ff*, it is sufficient to compute the maximum frequency (f_{max}) (corresponding to $ff \to 1$) from the electrical model to describe a linear function using all the known elements:

$$f_{osc} = \frac{f_{osc.\max} - f_{osc.\min}}{ff_{\max} - f_{\min}} \cdot ff + f_{osc.\min} \tag{9}$$

where $ff_{max} = 1$ and $ff_{min} = 0$. Then, we have that:

$$f_{osc} = (f_{osc.\max} - f_{osc.\min}) \cdot ff + f_{osc.\min} \tag{10}$$

which can be rewritten and solved for *ff*:

$$ff = \frac{f_{osc} - f_{osc.\min}}{f_{osc.\max} - f_{osc.\min}} \tag{11}$$

where f_{osc} corresponds to the frequency experimentally measured and *ff* is the estimated *fill factor*.

IV. RESULTS

In this section, we report the results for each estimation method. As a comparison metric, we obtained the cell concentration, i.e., N_{cell}/cm^2, obtained by traditional methods, optically counting the number of cells with the Leica DMI1 inverted microscopy every 24h until the confluence phase was reached. The cell concentration (N_{con}) was obtained by using *ff* in Equation (12) below.

Traditional cell counting was obtained as the mean of 3 counting samples. This traditional counting method provides an error margin. We estimated the cell area for the upper and lower margins of this traditional counting method to obtain the cell-density error margin in the *MSE* and *DPM* methods.

$$N_{con} = \frac{N_{cell}}{A_{well}[cm^2]} \text{ where } N_{cell} = \frac{A_{well}}{A_{cell}} \times ff \tag{12}$$

where N_{cell} is the cell number in the well at any arbitrary moment, A_{well} is the well area, and A_{cell} is the mean cell area. In our case, we considered that $r_{cell} = 13.3\mu$m.

A. Minimization of System Equations

Results related to the MSE method are depicted in Fig. 9. Note that for each initial cell number, the error was very small. Indeed, for the greatest initial cell number, the error was minimum (10.000 is a very small cell number). The initial error was not acknowledged given that it was caused by some perturbations resulting from the adaptation of the cells to the wells and deviations of temperature, humidity, and CO_2 from their ideal values. These deviations were due to the opening of the incubator; they were corrected after a few hours. Note that, for initial cell numbers of 5.000 and 10.000, the error ranges of the traditional counting method and *MSE* were similar after 48 hours from the starting point of the experiment until the end.

B. Dataset Predictive Model

For *DPM*, Fig. 9 illustrates the prediction for the same experimental values as in the previous method. The resulting curves provide good matching with the experimental ones. There exists some dispersion probably due to the electrode shape and sensing surface. For most of the results, the mean

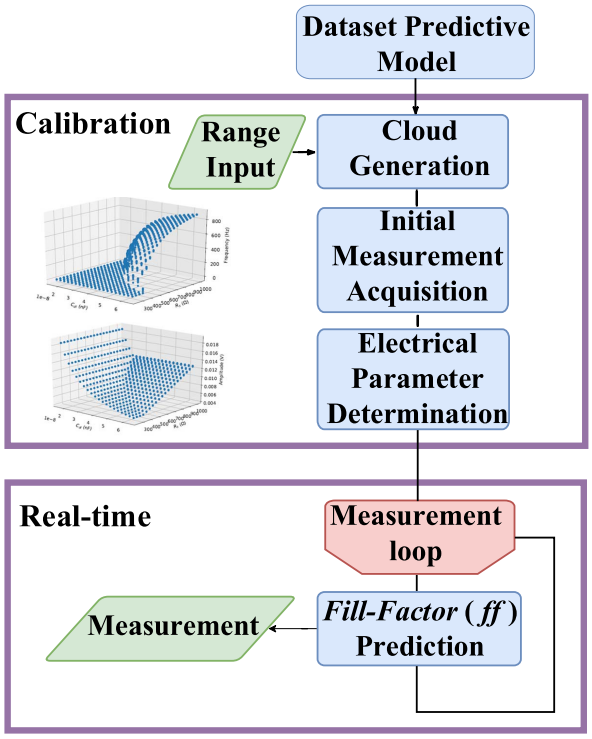

Fig. 5. Flowchart of the DPM method. This flowchart depicts the steps needed to estimate the value of *ff* using the DPM method. The algorithm generates a dataset for potential experimental results using the analytical sensor model. This dataset encodes a function of f_{osc} and a_{osc} with respect to variations on electrical parameters (such as those introduced by the electrodes). An estimate of such electrical parameters is performed from the initial measurements acquired to enable real-time prediction of different *ff* values.

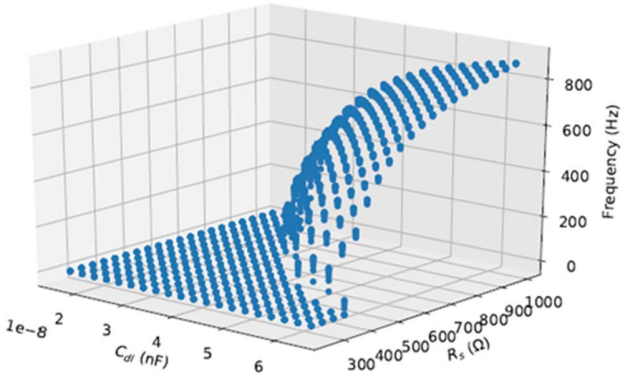

Fig. 6. Frequency dataset for variation of the electrical parameters C_{dl} and R_S.

value of the cell radius estimation (blue line) is evaluated within statistical significance with respect to traditional counting methods (which may have a certain dispersion in some measurements).

C. Comparison

Both methods provided a good enough estimation of the cell concentration. By comparing Fig. 9 and Fig. 8, we can see that *DPM* was better for a low initial cell number and for the first hours of the experiment, while the *MSE* method was

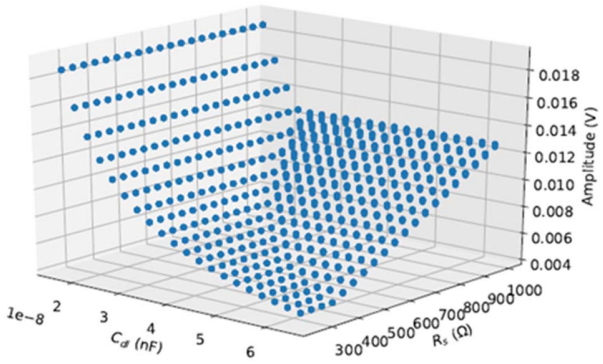

Fig. 7. Amplitude dataset for variation of the electrical parameters C_{dl} and R_S.

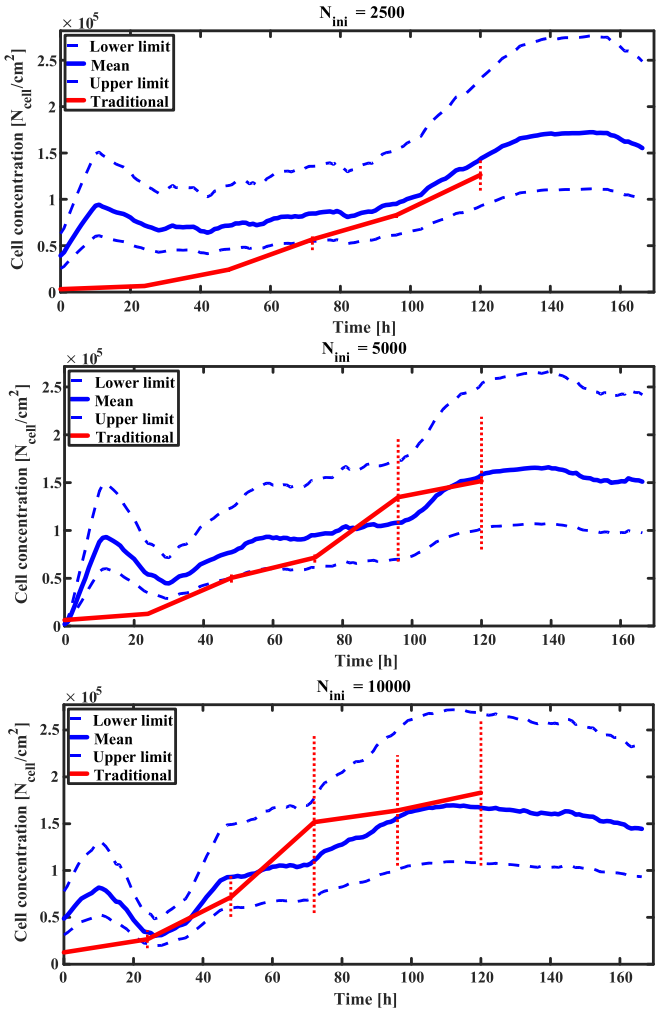

Fig. 8. Comparison of cell concentration between traditional methods and the *DPM* method for three initial cell numbers (2500, 5000, and 10000 cells), where the red line represents the traditional counting method with its error range (vertical red line), and the blue line represents the estimation of cell concentration using the *DPM* method with its error range (blue dashed lines).

better for a higher initial cell number and from the middle to the end of the experiment.

TABLE II shows the mean relative errors of both methods with respect to traditional counting in row $e_{\mathbf{r}}$. The relative

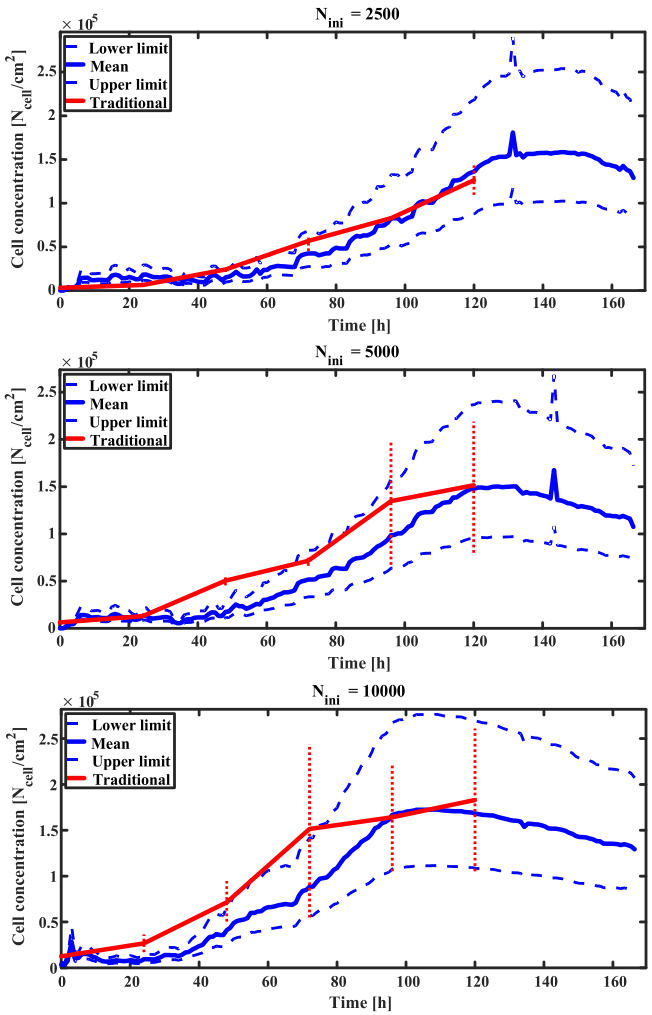

Fig. 9. Comparison of cell concentration between traditional methods and the MSE method for three initial cell numbers (2500, 5000, and 10000 cells), where the red line represents the traditional counting method with its error range (vertical red line), and the blue line represents the estimation of cell concentration using the MSE method with its error range (blue dashed lines).

TABLE II
RELATIVE ERROR

N_{ini} [cells]	2.500		5.000		10.000	
Method	*MSE*	*DPM*	*MSE*	*DPM*	*MSE*	*DPM*
$\overline{e_r}$	0.31	0.11	0.18	0.15	0.13	0.14
$\overline{e_r}$ *(ff < 0.5)*	0.37	0.09	0.19	0.13	0.17	0.11
$\overline{e_r}$ *(ff ≥ 0.5)*	0.17	0.17	0.16	0.19	0.09	0.17

error was estimated through the next equation:

$$\overline{e_r} = \frac{1}{n}\sum_{i=1}^{n}\left(\frac{|N_{con.method}(i) - N_{con.trad}(i)|}{N_{con.trad}(i)}\right) \qquad (13)$$

where $\overline{e_r}$ is the mean relative error, $N_{con.method}$ and $N_{con.trad}$ denote the cell concentration vectors estimated by each method and by traditional counting, respectively, and n is the number of samples employed to estimate $\overline{e_r}$. The first row shows the mean relative error of the whole experiment. The next rows show the mean relative error when *ff* was less than 0.5 and greater or equal than 0.5, respectively. The *MSE* method provided better estimates of cell concentration when *ff* was greater than 0.5 and for experiments whose initial cell numbers were high. By contrast, the *DPM* method provided better estimates of cell concentration when *ff* was lower than 0.5 and for experiments whose initial cell numbers were low.

V. CONCLUSIONS

Two analytical methods were proposed in this study to obtain the evolution of cell concentration in a growth experiment of CC assay. Previous methods reported by the authors [16] apply an estimation algorithm which requires the full experiment information to be able to perform estimation. The proposed methods allow to estimate the cell concentration during the experiment (in real-time) without having to wait until the end of the experiment. The ECIS technique, along with the electrical model of an electrode in a saline solution, were applied to estimate the bioimpedance of a CC assay in each well and the *ff* parameter, thereby achieving real-time prediction of the cell density present in the assay.

Each method has a working zone, defined by the experiment progress and initial cell concentration, where it is more accurate. A comparison of the ranges of both methods (Fig. 9 and Fig. 8, in dashed blue line) with the ranges of traditional counting (Fig. 9 and Fig. 8, in dashed red line) shows that the proposed methods achieve positive results. In addition TABLE II reports the error and the best working zone of each method in order to evaluate their accuracy.

The parameters R_{gap} and ΔR_s do not affect when *ff* is low [16]. The *MSE* method was less accurate in this part of the experiment given that it estimates these parameters for each measurement. By contrast, when *ff* is high, R_{gap} and ΔR_s affect the most (their estimations are more accurate) and thus the estimation of *ff* (and cell concentration) is more accurate.

The *DPM* method is based on a previous estimation of the cell-electrode model parameters. This estimation provides a very accurate estimation of the *ff* when this parameter is low, given that R_{gap} and ΔR_s do not affect in the interval ranging from the beginning to the middle of the experiment. When the *ff* was high, small errors in the value of R_{gap} and ΔR_s could cause a decrease in accuracy.

For this reason, we conclude that the combination of both methods can probably result in a general procedure for more accurate estimates of the cell concentration at any point of the experiment without prior calibration. According to the results obtained, we consider that using the *DPM* method when the estimated *ff* is low and the *MSE* method for *ff* greater than a certain value, in particular when $ff > 0.5$, can give rise to a better fitting method. For future experiments, both methods will be combined and their accuracy and operation will be verified.

APPENDIX

Below are the equations obtained by calculating the real and imaginary parts in Equation (4). Note that *eq1* and *eq2*

are Equations (1) and (2) in this appendix.

$$\mathrm{Re}(1+H_{BP}(s)\cdot H_Z(s)\cdot H_{CMP.F}(s)\cdot N(a_{osc},\varpi_{osc}))=0 \quad (1)$$

$$\mathrm{Im}(1+H_{BP}(s)\cdot H_Z(s)\cdot H_{CMP.F}(s)\cdot N(a_{osc},\varpi_{osc}))=0 \quad (2)$$

where $s = j\cdot\omega_{osc}$, H_Z is the transfer function of the cell-electrode electrical model; H_{BP} and $H_{CMP.F}$ are the transfer functions of the band-pass filter and the pre-comparator filter of the *OBT* system, respectively; and $N(a_{osc}, \omega_{osc})$ is the comparator describing function of the *OBT system* [20]. Estimates of $N(a_{osc}, \omega_{osc})$, H_{BP}, and $H_{CMP.F}$ are reported in [16].

Acknowledgment

The authors would like to thank Dr. Paula Daza and Maria Esther Martin, from D. of Cell Biology, Faculty Biology of the Universidad de Sevilla, for their valuable help and supervision on cell culture implementation, discussion, and comments.

References

[1] R. I. Freshney, *Culture of Animal Cells: A Manual of Basic Technique and Specialized Applications*, 6th ed. Hoboken, NJ, USA: Wiley, 2011.
[2] *Applied Biophysics*. Accessed: Jul. 28, 2020. [Online]. Available: http://www.biophysics.com/
[3] S. Schmidt *et al.*, "Microwave induced electroporation of adherent mammalian cells at 18 GHz," *IEEE Access*, vol. 7, pp. 78698–78705, 2019.
[4] M.-H. Jun *et al.*, "Glucose-independent segmental phase angles from multi-frequency bioimpedance analysis to discriminate diabetes mellitus," *Sci. Rep.*, vol. 8, no. 1, p. 648, Dec. 2018.
[5] F. A. Alexander, D. T. Price, and S. Bhansali, "From cellular cultures to cellular spheroids: Is impedance spectroscopy a viable tool for monitoring multicellular spheroid (MCS) drug models?" *IEEE Rev. Biomed. Eng.*, vol. 6, pp. 63–76, 2013.
[6] R. C. Nordberg, J. Zhang, E. H. Griffith, M. W. Frank, B. Starly, and E. G. Loboa, "Electrical cell-substrate impedance spectroscopy can monitor age-grouped human adipose stem cell variability during osteogenic differentiation," *STEM CELLS Transl. Med.*, vol. 6, no. 2, pp. 502–511, Feb. 2017.
[7] C.-L. Hsu, A. Sun, Y. Zhao, E. Aronoff-Spencer, and D. A. Hall, "A 16×20 electrochemical CMOS biosensor array with in-pixel averaging using polar modulation," in *Proc. IEEE Custom Integr. Circuits Conf. (CICC)*, Apr. 2018, pp. 1–4.
[8] D. Rego, L. Costa, M. T. Pereira, and L. M. Redondo, "Cell membrane permeabilization studies of Chlorella sp. By pulsed electric fields," *IEEE Trans. Plasma Sci.*, vol. 43, no. 10, pp. 3483–3488, Oct. 2015.
[9] I. Giaever and C. R. Keese, "Use of electric fields to monitor the dynamical aspect of cell behavior in tissue culture," *IEEE Trans. Biomed. Eng.*, vol. BME-33, no. 2, pp. 242–247, Feb. 1986, doi: 10.1109/tbme.1986.325896.
[10] I. Giaever and C. R. Keese, "Micromotion of mammalian cells measured electrically," *Proc. Nat. Acad. Sci. USA*, vol. 88, no. 17, pp. 7896–7900, 1991, doi: 10.1073/pnas.88.17.7896.
[11] P. Daza, A. Olmo, D. Cañete, and A. Yufera, "Monitoring living cell assays with bio-impedance sensors," *Sens. Actuators B, Chem.*, vol. 176, pp. 605–610, Jan. 2013, doi: 10.1016/j.snb.2012.09.083.
[12] R. Pradhan, A. Mitra, and S. Das, "Characterization of electrode/electrolyte interface of ECIS devices," *Electroanalysis*, vol. 24, no. 12, pp. 2405–2414, Dec. 2012, doi: 10.1002/elan.201200455.
[13] P. Pérez *et al.*, "Sensing cell-culture assays with low-cost circuitry," *Sci. Rep.*, vol. 8, no. 1, p. 8841, Dec. 2018.
[14] X. Huang, D. Nguyen, D. W. Greve, and M. M. Domach, "Simulation of microelectrode impedance changes due to cell growth," *IEEE Sensors J.*, vol. 4, no. 5, pp. 576–583, Oct. 2004.
[15] J. Wissenwasser, M. J. Vellekoop, and R. Heer, "Signal generator for wireless impedance monitoring of microbiological systems," *IEEE Trans. Instrum. Meas.*, vol. 60, no. 6, pp. 2039–2046, Jun. 2011.
[16] J. Serrano *et al.*, "An empirical-mathematical approach for calibration and fitting cell-electrode electrical models in bioimpedance tests," *Sensors*, vol. 18, no. 7, p. 2354, Jul. 2018.
[17] E. García, P. Pérez, A. Olmo, R. Díaz, G. Huertas, and A. Yufera, "Data-analytics modeling of electrical impedance measurements for cell culture monitoring," *Sensors*, vol. 19, no. 21, p. 4639, Oct. 2019.
[18] M. Parsian, *Data Algorithms*. Newton, MA, USA: O'Reilly Media, 2015.
[19] D. A. Borkholder, "Cell based biosensors using microelectrode," Ph.D. dissertation, Dept. Elect. Eng., Stanford Univ., Stanford, CA, USA, 1998.
[20] G. Huertas, D. V. García de la Vega, A. Rueda, and J. L. Huertas, *Oscillation-Based Test in Mixed-Signal Circuits*. Dordrecht, The Netherlands: Springer, 2006.
[21] J. Nocedal and S. J. Wright, *Numerical Optimization*. New York, NY, USA: Springer, 2006.